Bioconjugate Chemistry

pubs.acs.org/bc Article

Supramolecular Encapsulation of Small-Ultrared Fluorescent Proteins in Virus-Like Nanoparticles for Noninvasive In Vivo Imaging Agents

Fabian C. Herbert, Olivia R. Brohlin, Tyler Galbraith, Candace Benjamin, Cesar A. Reyes, Michael A. Luzuriaga, Arezoo Shahrivarkevishahi, and Jeremiah J. Gassensmith*

Cite This: *Bioconjugate Chem.* 2020, 31, 1529−1536 Read Online

ABSTRACT: Icosahedral virus-like particles (VLPs) derived from bacteriophages Qβ and PP7 encapsulating small-ultrared fluorescent protein (smURFP) were produced using a versatile supramolecular capsid disassemble−reassemble approach. The generated fluorescent VLPs display identical structural properties to their nonfluorescent analogs. Encapsulated smURFP shows indistinguishable photochemical properties to its unencapsulated counterpart, exhibits outstanding stability toward pH, and produces bright in vitro images following phagocytosis by macrophages. In vivo imaging allows the biodistribution to be imaged at different time points. Ex vivo imaging of intravenously administered encapsulated smURFP reveals a localization in the liver and kidneys after 2 h blood circulation and substantial elimination after 16 h of imaging, highlighting the potential application of these constructs as noninvasive in vivo imaging agents.

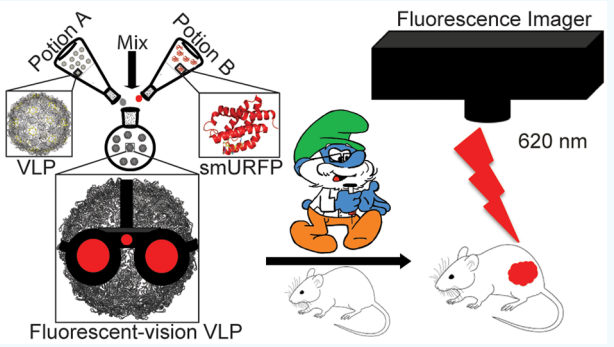

INTRODUCTION

Soft proteinaceous nanoparticles derived from the capsids of bacteriophages or plants have emerged as promising technologies[1] in imaging[2,3] and drug delivery[4−7] and as noninfectious models in vaccine development.[4,6,8−14] In particular, virus-like particles (VLPs)—engineered nanostructures that self-assemble from individual coat proteins (CPs) of a virus—are structurally similar to their viral analogs but lack the genetic material needed for replication.[15] VLPs can be expressed in a scalable and straightforward fashion in a variety of systems including insect cells, mammalian cells, and bacteria.[16] Further, VLPs are characterized by polyvalency—they are high-symmetry quaternary structures with functional handles that facilitate multiple orthogonal surface functionalizations.[17−22] This chemical flexibility and their biocompatibility and biodegradability[9] have allowed VLPs to serve as multivalent platforms for the conjugation of therapeutics,[23] pH-cleavable groups,[6,24] and fluorescent dyes.[19,25−28] This emerging utility has necessitated a straightforward way to visualize the VLPs both in vivo and in vitro. The typical strategies to afford fluorescent VLPs for cell and animal imaging have involved bioconjugation of synthetic dyes, which can be expensive, will occupy valuable reactive residues on protein surfaces, and can alter their structure and antigenicity.[29] Noncovalent methods of dye conjugation are sparse, though several elegant methods using genetically encoded protein−peptide interactions have produced a modular method to encapsulate green fluorescent protein (GFP) within the hollow capsid of viral nanoparticles.[30,31] Here, we utilize a supramolecular strategy to capture a proteinaceous far-red fluorescent probe for the production of near-infrared fluorescent VLPs (Scheme 1).

Far-red fluorescent proteins (FPs) have become desirable platforms as in vivo imaging agents, offering new alternatives to dyes and metal nanoparticles for the advancement of real-time imaging of tissue.[32−34] These probe's spectral properties lay in an optical window free of interaction between incident light and predominant endogenous molecules such as water or hemoglobin, resulting in reduced autofluorescence and better tissue penetration.[35] FPs with absorbance maxima around 650 nm can be excited with red lasers (Cy5) commonly found in confocal microscopes, fluorescence-activated cell sorters, and flow cytometers, making them ideal platforms for in vitro imaging.[35,36] Recently, a far-red fluorescent protein was developed from the allophycocyanin α-subunit (APCα)[37,38] called small-ultrared fluorescent protein (smURFP), which was

Received: April 2, 2020
Revised: April 27, 2020
Published: April 28, 2020

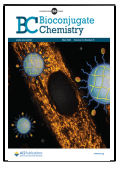

https://dx.doi.org/10.1021/acs.bioconjchem.0c00190
Bioconjugate Chem. 2020, 31, 1529−1536

Scheme 1. Representation of the Disassembly−Reassembly Process Used for Synthesis of Far-Red Fluorescent Virus-Like Particles[a]

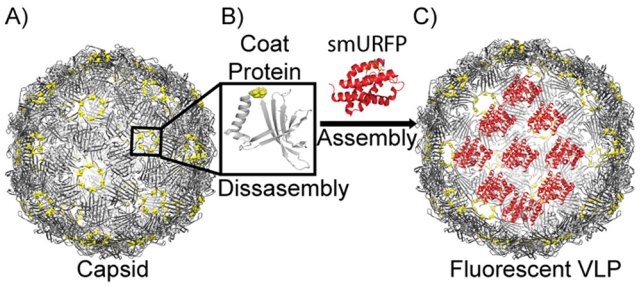

[a](A) Chimera crystal structure of native PP7. (B) Isolated coat protein obtained after incubation of VLPs in urea, dithiothreitol, and tris-hydrochloride. (C) Far-red fluorescent VLPs packed with smURFP.

genetically tuned to incorporate biliverdin (BV), a tetrapyrrolic bile pigment ubiquitous to mammalian cells.[39] As a result, smURFP displays excitation/emission maxima of 642/670 nm, matching the organic reporter group Cy5, making it compatible with filter sets on modern fluorescent microscopes and animal imaging stations. Other far-red/near-infrared (NIR) FPs have been engineered from bacterial phytochromes to incorporate BV but are typically less stable and have lower overall brightness.[40,41] smURFP is the brightest of proteins derived from allophycocyanin capable of imaging within the near-infrared tissue window, possessing the highest extinction coefficient (180 000 M^{-1} cm^{-1}) and quantum yield (~18%).[42] Indeed, this FP displays comparable brightness to enhanced green-fluorescent protein (eGFP) and at least 2-fold brighter than most coral-derived far-red fluorescent proteins. Unlike GFP, smURFP is not pH sensitive,[43] making it useful for live-cell imaging where the probe may end up in an acidic organelle like an endosome or a lysosome.

Engineered VLPs from the family *Leviviridae*—including bacteriophage Qβ, bacteriophage MS2, and pseudomonas phage seven (PP7)—have emerged as prototypical VLP nanotechnology platforms and are structurally similar. The "inner surface" of the coat protein has a positive charge, which binds to random RNA, in turn directing formation of intact capsids during recombinant expression in *E. coli*. This positive charge has been exploited to allow disassembled MS2 phage coat proteins to reassemble around negatively charged cargo, typically with the aid of osmolytes.[44,45] Further, this charge-mediated assembly strategy has also been employed in other VLP systems such as Cowpea Chlorotic Mottle Virus (CCMV) and in lumazine synthase, an enzyme responsible for biosynthesis of riboflavin.[46,47] Given that the APCα subunit has an isoelectric point[48] of 4.64, we suspected smURFP would act as a template for the reassembly of other *Leviviridae* capsids at neutral pH. In this report, we show that a disassembly followed by templated reassembly approach permits the encapsulation of smURFP inside both Qβ and PP7 in good yield, producing bright fluorescent complexes referred to as S@Qβ and S@PP7, respectively. The resulting far-red fluorescent VLPs are indistinguishable in size to nonfluorescent VLP analogs. Further, the supramolecular constructs display identical photochemical properties to native smURFP. Finally, we show both constructs to be effective noninvasive in vivo imaging agents when injected subcutaneously and intravenously.

RESULTS AND DISCUSSION

Both Qβ and PP7 are highly functionalizable, monodisperse, biocompatible, and biodegradable icosahedral VLPs that range between 26 and 28 nm and are composed of 180 identical coat proteins.[50,51] These building units self-assemble around the negative charge of single-stranded RNA and are joined together through disulfide bonds formed between pairs of surface-exposed cysteines present in each coat protein. Control over the self-assembly properties of these VLPs can be exploited for the encapsulation of foreign material within their hollow capsid,[52,53] though, to our knowledge, this self-assembly has not been exploited to form fully proteinaceous near-IR imaging agents.

Supramolecular encapsulation of smURFP within the hollow interior of the VLPs is straightforward and carried out via disassembly of the capsids upon incubation in a reducing solution—to reduce the 180 disulfides on either capsid—and at low pH and high salt concentration. Particle reassembly is achieved through incubation of the concentrated VLP monomers in the presence of 10-fold molar excess of smURFP at neutral pH. smURFP protein production is very straightforward and can be expressed in large (gram) quantities in the laboratory,[38] thus permitting a stoichiometric excess during its use as a template. The whole synthesis is relatively efficient, and we were able to obtain a ~65% yield of S@VLP after purification. The purified blue suspension exhibited red emission under UV light (Figure 1A) and shows a uniform size distribution with comparable sizes to native and fluorescent VLPs by dynamic light scattering (DLS) (Figure 1B). Reassembly and morphology of the capsids was further confirmed by transmission electron microscopy (TEM) (Figure 1C and 1D), which showed no differences in the morphology between fluorescent and native VLPs (TEM micrographs of native Qβ and PP7 are found in SI Figure S1A and S1B). From this, we conclude that the disassembly−reassembly approach does not result in any alteration or morphological difference of the proteinaceous nanocarriers used for our study.

To examine the fluorophore intactness of the assembled fluorescent VLPs, ultraviolet−visible (UV−vis) and fluorescence spectroscopy were performed. As expected, long-wavelength absorption with λ_{max} of 642 nm and fluorescence emission λ_{max} of 670 nm between native and encapsulated smURFP display identical spectral properties (Figure S1C and S1D). To verify smURFP encapsulation within the capsids, FPLC and gel electrophoresis were performed and compared to the respective native analogs (Figure 2). Overlapping absorbance recorded at 280 and 642 nm reveals the presence of smURFP within the capsids of both Qβ and PP7 (Figure 2A and 2B), which elute very early (12 mL) on our column. Native smURFP elutes later (20 mL), and samples of S@VLP contained no free smURFP per FPLC, confirming no particle leakage from within the capsids. While the constructs are stable for over 1 week in the refrigerator, long-term stability of S@Qβ and S@PP7 is still an area of ongoing research. Agarose electrophoretic mobility exhibits similar band positions between native and fluorescent VLPs when stained with Coomassie Brilliant Blue. Fluorescence gel imaging in the Cy5 channel shows only S@Qβ and S@PP7 bands with shifts matching the mobility observed with Coomassie (Figure 2C).

https://dx.doi.org/10.1021/acs.bioconjchem.0c00190
Bioconjugate Chem. 2020, 31, 1529−1536

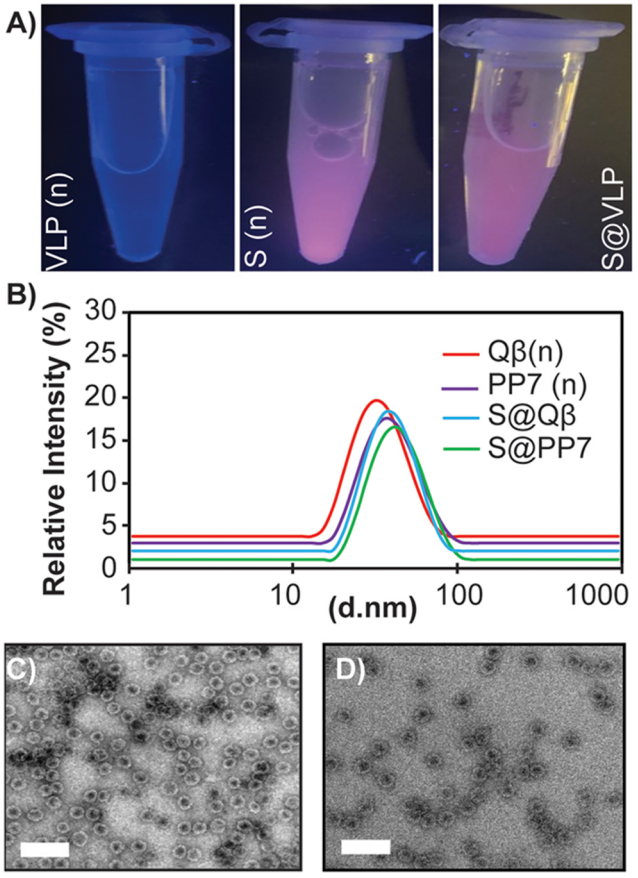

Figure 1. Characterization of smURFP@VLPs. (A) Photograph of VLP samples irradiated by a hand-held UV lamp (350 nm) before and after encapsulation of smURFP. (B) DLS of unmodified (native) and fluorescent VLPs. TEM micrographs of (C) S@Qβ and (D) S@PP7. Scale bar = 100 nm.

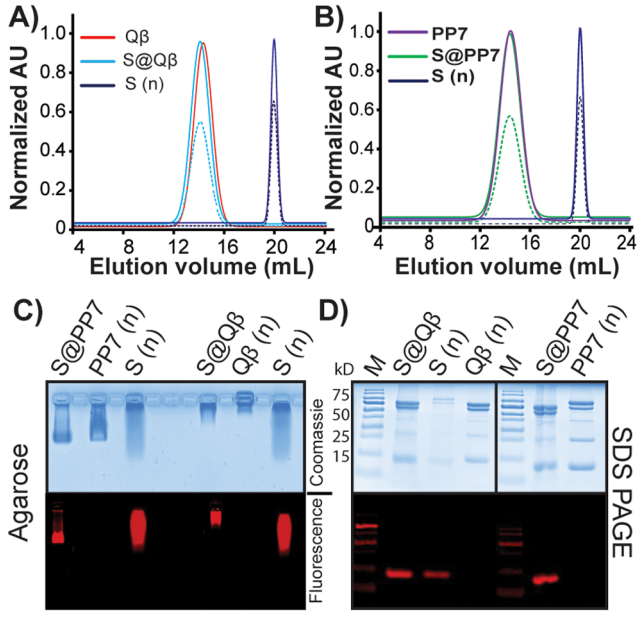

Figure 2. Chromatography and gel electrophoresis characterization of S@VLPs. (A) FPLC elution volumes of native Qβ, S@Qβ, and native smURFP (S (n)). Solid lines were recorded at 280 nm, and dotted lines were recorded at 640 nm. (B) FPLC elution volumes of native PP7, S@PP7, and S (n). Solid lines were recorded at 280 nm, and dotted lines were recorded at 640 nm. (C) Agarose of fluorescent VLPs, native capsids, and native smURFP. Top gel stained in blue shows protein bands imaged under Coomassie Brilliant Blue.

Nonreducing SDS-PAGE confirms the previous results, which shows the fluorescent proteins. Because the CP of both VLPs and smURFP are approximately 15 kDa, the bands appear to have similar electrophoretic mobilities by SDS PAGE (Figure 2D). smURFP is also known to form higher order aggregates,[54] which are also visible; however, fluorescence gel imaging in the Cy5 channel reveals signal only from monomeric smURFP.

Gel densitometry was used to quantify the concentration of smURFP present in both Qβ and PP7 capsids. Ten percent nonreducing SDS PAGE was used to highlight the protein band pertaining to either the monomer unit of the VLP or smURFP. Varying concentrations of native smURFP and native Qβ or PP7 were run in tandem with S@Qβ and S@PP7 (Figure S2). Standard curves made from the protein band absorbances were constructed. From these data we conclude that there are approximately three smURFP per VLP, a result that is in line with the literature[45] that used a similar templating strategy to capture GFP inside MS2.

Early elegant work[30] that produced GFP-encapsulated Qβ using a different approach placed an RNA aptamer and a Qβ packing hairpin on Qβ CPs, which facilitated the interaction of Rev peptide-tagged GFP during VLP self-assembly. While the probe behaved well generally and we published using this exact construct in the past,[6] we found live imaging difficult because of GFP's well-known sensitivity to low pH.[55] In particular, we found image living cells once the particles entered into late endosomes nearly impossible. smURFP, in contrast, has been shown to be relatively insensitive to pH, giving us hope that we could use this as a more pH-independent system for live-cell imaging. Like GFP, the optical properties of smURFP align with the filter sets for Cy5, ubiquitous on modern imaging instruments. Before incubation in cells, we tested the stability of smURFP and S@VLPs against an array of pH values and compared them directly to GFP analogues. The recorded fluorescence intensity for smURFP, whether encapsulated or native, shows no quenching from pH 4 to 8 (Figure 3A). On the contrary, encapsulated and native GFP display significant quenching when incubated at pH 3−5 (Figure 3B), suggesting smURFP would be a better platform for in vitro imaging applications where the nanoparticle carriers would end up in the late endosomes and/or lysosomes.[28] To test this, a qualitative evaluation of VLP formulations prepared with GFP (G@VLP) and smURFP (S@VLP) was done via live-cell imaging. Fluorescent VLPs incubated with RAW-264.7 macrophages for 4 h show successful internalization for all systems. Importantly, data obtained from this study show that, at the same fluorophore concentrations and identical laser powers,[56] the smURFP-containing VLPs were close to saturating the detector and clear puncta can be observed whereas the poorly resolved GFP analogue (Figure 3 C−F) is faintly visible in only some cells. These results are even more clear in the reconstructed Z-stacks (Supporting Information movies).

Next, we sought to test the in vivo performance of our new constructs. smURFP's optical properties lend it utility in near-infrared imaging through tissue. Recent work by Rodriguez and Ting[39] showed that smURFP-BSA nanoparticles produce fluorescence bright enough to image tumors in live murine models. While it is not the most red shifted of the new ultrared

https://dx.doi.org/10.1021/acs.bioconjchem.0c00190
Bioconjugate Chem. 2020, 31, 1529−1536

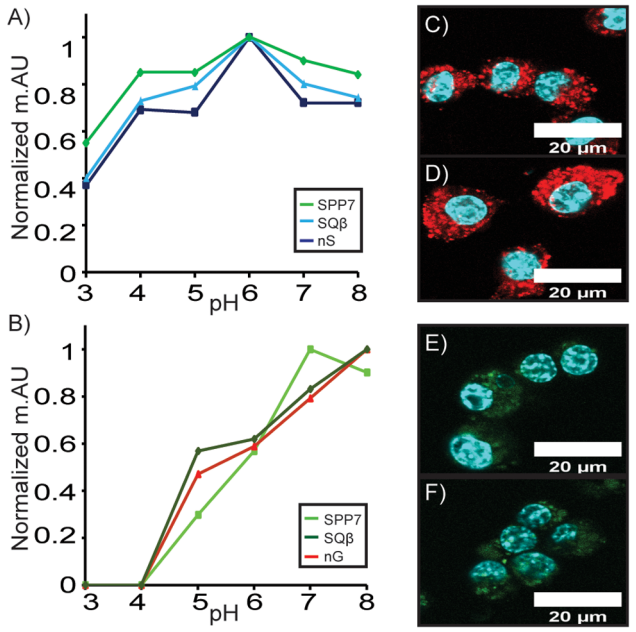

Figure 3. pH-responsive studies and live-cell imaging characterization of smURFP and GFP@VLPs. (A) Emission spectra of smURFP@VLPs and native smURFP obtained at λ_{max}670 nm under varying pH values. (B) Emission spectra of GFP@VLPs and native GFP obtained at λ_{max}509 nm at varying pH values. (C) S@PP7 incubated in RAW 264.7 macrophages (4 h). Color code: blue, DAPI; red, Cy5. (D) S@Qβ incubated in RAW 264.7 macrophages (4 h). Color code: blue, DAPI; red, Cy5. (E) G@PP7 incubated in RAW 264.7 macrophages (4 h). Color code: blue, DAPI; green, GFP. (F) G@Qβ incubated in RAW 264.7 macrophages (4 h). Color code: blue, DAPI; green, GFP. Scale bar = 20 μm.

proteins, it is the brightest,[37] and we thus expected to visualize the probe in living animals following subcutaneous and intravenous injections.

First, we wanted to establish if the probe was visible under the skin at all. Prior to injection, the torso and limbs of the mice were shaved. Fluorescent samples were administered subcutaneously and monitored for 8 h (Figure 4A). We can also see that the capsids themselves show no fluorescence, even when imaged just under the skin, indicating that all fluorescence signal arises from the smURFP. The larger VLP formulations resided in the tissue for more than 4 h but had completely diffused from the area by 8 h. smURFP by itself, on the other hand, diffused from the injection site almost entirely at 4 h (Figure 4B).

Next, we wanted to see if we could observe the internal anatomy with our probe. Intravenous (tail vein) administration was likewise successful. We were able to distinguish both kidneys—the typical presentation of the right kidney positioned lower than the left—in depilated mice in the supine position after 120 min (Figure 4C, left). Ex vivo imaging (Figure 4C, right) confirms both kidneys and the liver contained probe with VLP formulations visible in the liver for as long as 16 h post injection (Figure S3). Injections of smURFP protein, on the other hand, were apparent in very minute quantities in the liver at 2 h (Figure 4D).

CONCLUSION

Using a versatile supramolecular disassembly−reassembly approach, we successfully encapsulated smURFP within the hollow capsids of two different VLPs—Qβ and PP7. The as-prepared fluorescent VLPs show size distributions and shapes consistent to their native analogs, as confirmed by DLS and TEM. Spectral properties between native and encapsulated smURFP were found to be very similar. When compared to

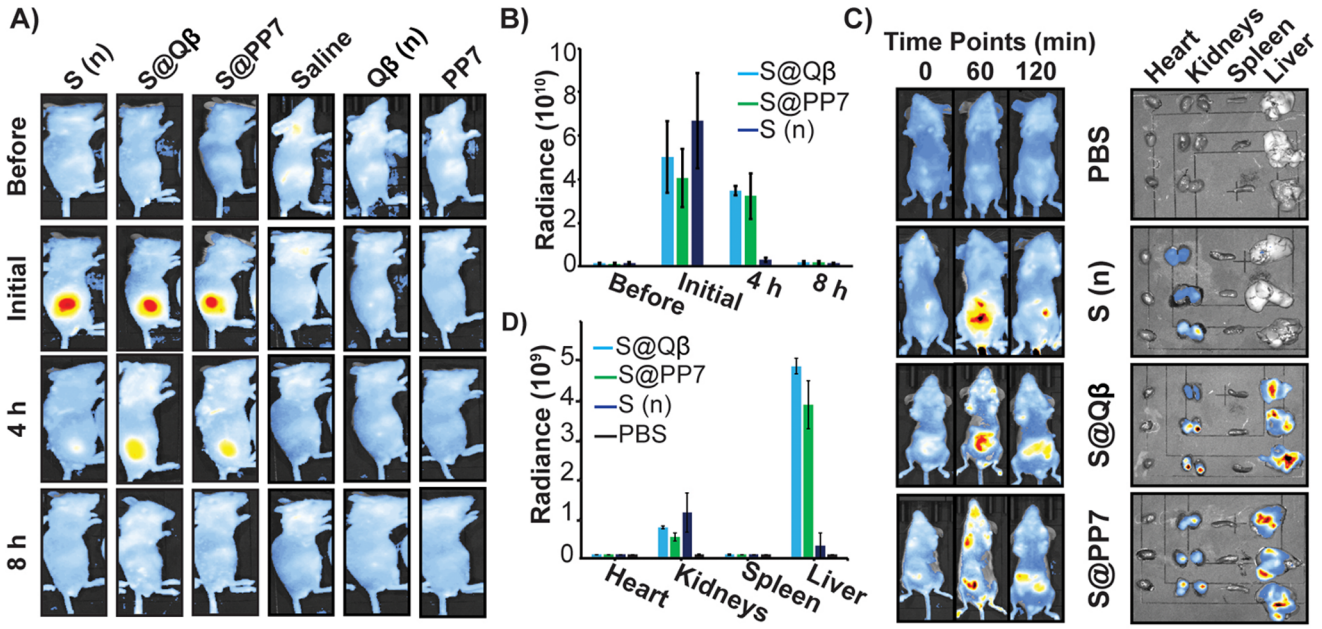

Figure 4. (A) Subcutaneous diffusion assay shows S@VLP formulations reside in the tissue longer than native smURRP, which is completely gone within 4 h. (B) Plot of fluorescence radiance of the subcutaneous injection. As expected, saline, PP7 (n) and Qβ (n) do not show any fluorescence. (C) Intravenous administration of PBS as a negative control, S (n), S@Qβ, and S@PP7 shows accumulation. Animals were imaged in the supine position show fluorescence kidneys and liver, ex vivo imaging of necropsied organs show localization in the liver for VLPs but not S (n). (D) Relative radiance at the time of sacrifice shows the principle location of accumulation is the liver and some in the kidney.

https://dx.doi.org/10.1021/acs.bioconjchem.0c00190
Bioconjugate Chem. 2020, 31, 1529−1536

GFP-loaded analogs, smURFP-loaded VLPs are easier to image following phagocytosis in RAW macrophages, which we attribute to the better pH sensitivity of smURFP. Finally, smURFP-encapsulated Qβ and PP7 could be clearly visualized in the skin and mice and showed different tissue and organ localization compared to free smURFP. We believe these results will be helpful in developing new ways to noninvasively track VLPs based on these constructs in tissue in a myriad of biomedical applications.[57]

EXPERIMENTAL SECTION

Materials and Chemicals. FBEssence, 2-methyl imidazole, potassium chloride, potassium phosphate monobasic, potassium phosphate dibasic, sodium phosphate monobasic, sodium phosphate dibasic, Dulbecco's Modified Eagle's Medium (6429), Tris base, tryptone, peptone, yeast extract, glycine, sodium dodecyl sulfate, Lowry modified reagent, and sodium chloride were purchased from Thermo Fisher Scientific (Waltham, MA, USA, Research Product International (Mt. Prospect, IL, USA), Chem-Impex Int'l (Wood Dale, IL, USA), VWR (Radnor, PA, USA), and Sigma-Aldrich (St. Louis, MO, USA). All reagents were used with no additional purification.

Protocol for Expression of Qβ and PP7. Expression and purification of VLPs were done following a reported procedure,[49] which is briefly described below. Both plasmids were kindly gifted by Prof. M.G. Finn from the Georgia Institute of Technology. Transformed single colonies of BL21 DE3 *E. coli* cells were incubated in 50 mL of SOB media supplemented with kanamycin (50 μg mL^{-1}) overnight at 37 °C and 210 rpm (5 × *g*). Cells were amplified in 2 L of media at 37 °C until OD600 ranged between 0.7 and 0.9. Expression proceeded by induction with 1 mM isopropyl β-D-1-thiogalactopyranoside (IPTG) for 12 h at 37 °C. Cells were harvested through centrifugation with a Fiberlite F10 rotor at 10 500 rpm (19 510 × *g*) for 30 min at 4 °C. Cell lysis was done using a cell homogenizer. The resulting lysate was centrifuged using a Fiberlite F10 rotor at 10 500 rpm (19 510 × *g*) for 60 min at 4 °C. The supernatant was extracted, and the protein precipitated using 2 M ammonium sulfate, performed in a rotisserie for 12 h at 4 °C. The precipitate was harvested by centrifugation with a Fiberlite F10 rotor at 10 500 rpm (19 510 × *g*) for 60 min at 4 °C, and the protein pellet was resuspended in 20 mL of potassium phosphate buffer (1 M, pH 7.0). Membrane-bound proteins and lipids were removed through organic extraction using equal volumes of *n*-butanol and chloroform. The aqueous layer containing the VLPs was purified through 10−40% sucrose gradients using a SW-28 rotor at 28 000 rpm (87 808 × *g*) for 8 h. The collected VLP fractions were pelleted by centrifugation using a Beckman Type Ti-45 rotor at 40 000 rpm (179 200 × *g*) for 4 h and resuspended in potassium phosphate buffer (1 M, pH 7.0).

Protocol for Expression of smURFP. pBad-smURFP-RBS-HO-1 was a gift from Erik Rodriguez and Roger Tsien (Addgene plasmid # 80341; RRID:Addgene_80341) and purified as described below. Starter cultures of *E. coli* BL21 cells harboring the plasmids were amplified in SOB media supplemented with 50 μg mL^{-1} ampicillin at 37 °C. Induction was performed at OD 0.7 with 1% L-arabinose for a minimum of 12 h. Cells were pelleted at 10 500 rpm (19 510 × *g*) for 30 min using a Sorvall LYNX 4000 centrifuge, resuspended in 1 × PBS pH 8, and lysed using a Microfluidics M-110P Microfluidizer. Cells were again centrifuged at 10 500 rpm (19,510 × *g*) for 1 h to remove cell debris. The supernatant was purified using an NGC Quest 10 FPLC equipped with a 5 mL Bio-Scale Profinity IMAC cartridge. The samples were loaded using 1 × PBS pH 8, washed with 10 mM imidazole in 1 × PBS, pH 8, and eluted with 200 mM imidazole in 1 × PBS, pH 8. smURFP-containing fractions were dialyzed against Milli-Q water for 3 days and lyophilized using a Labconco Freezone 2.5 Lyophilizer. Dried smURFP was stored at 4 °C.

Protocol for Encapsulation of smURFP in VLPs. "Native" VLPs (10 mg mL^{-1}) were incubated in a disassembly solution consisting of 10 mM dithiothreitol, 20 mM Tris-HCl, 6 M urea, and 50 mM NaCl for 5 h at 4 °C with moderate stirring. Coat proteins pertaining to disassembled VLPs were harvested by centrifugation using a Fiberlite F10 rotor at 10 500 rpm (19 510 × g) for 30 min at 4 °C. The supernatant was dialyzed against 50 mM NaCl and 10 mM acetic acid for 12 h using a 3.5 kDa dialysis bag. Excess salts were removed from the coat proteins through a Sephadex G-25 column that had previously been equilibrated with potassium phosphate buffer (1 M, pH 7.0). The collected fraction was concentrated using a 10 kDa molecular-weight cutoff (MWCO) spin filter for 30 min at 4300 rpm (2071 × *g*). Further, coat proteins were combined with a 10-fold molar excess of fluorescent protein in a 10 mL glass vial and stirred for 30 min at 4 °C. Using a 3.5 kDa dialysis bag, fluorescent VLPs were then assembled by incubating the coat proteins and FP in a reassembly buffer consisting of 50 mM NaCl, 20 mM Tris-HCl (pH 7.5), 4 °C. For optimization of the encapsulation efficiency, the reassembly buffer was changed every 12 h (2 L) for a total cycle of 48 h. Further, the fluorescent VLPs were incubated in a 7 mM solution of hydrogen peroxide for 1 h to promote cysteine oxidation and full encapsulation of smURFP within the capsid. It is noteworthy that cysteine oxidation played a crucial role in our disassembly−reassembly process because without treatment in hydrogen peroxide the cargo would leak out of both Qβ or PP7 as observed by fast-protein liquid chromatography (FPLC). Excess salts were removed by passing the fluorescent VLPs through a 10 cm Sephadex G-25 column that had previously been equilibrated with potassium phosphate buffer (1 M, pH 7.0). Every milliliter of VLP loaded into the column required ∼2.5 mL of buffer to elute. Fully assembled fluorescent capsids were harvested through centrifugation using a 100 kDa MWCO spin filter for 30 min at 4300 rpm (2071 × *g*). On a similar experiment native VLPs were disassembled and dialyzed, and the coat proteins were isolated. The assembly of VLP coat proteins in the absence of cargo resulted in no capsid formation.

Fluorescent Virus-Like Particle Characterization. Protein concentration was assessed through Lowry Modified Assay (ThermoFisher Scientific) using bovine serum albumin as the internal standard. Homogeneity and purity of fluorescent VLPs were measured with TEM, SEC, and DLS. All fluorescent particles were icosahedral in shape, monodispersed in size, and eluted between 12 and 16 mL from a Superose-6 SEC column using potassium phosphate buffer (1 M, pH 7.0) as the mobile phase at a flow rate of 0.5 mL min^{-1} and absorbance measurements at 280/642 nm, respectively. Dynamic light scattering dynamic radii were recorded using potassium phosphate buffer (1 M, pH 7.0) and a protein concentration of 0.1 mg mL^{-1}. Spectral properties of each fluorescent VLP were recorded using native smURFP as control. The average number of encapsulated smURFP within the VLPs was assessed through gel densitometry, normalizing the dimer bands for the VLPs to estimate the concentration of

https://dx.doi.org/10.1021/acs.bioconjchem.0c00190
Bioconjugate Chem. 2020, 31, 1529−1536

Qβ or PP7 present in solution. This was complemented with UV−vis, in which long-wavelength absorption values at 642 nm were used to determine the concentration of smURFP present inside the VLP. From this analysis we found that each VLP contained ∼3 smURFP proteins housed in the interior of the capsid.

Live-Cell Imaging. RAW Macrophage 264.7 cells were cultured in Dulbecco's Modified Eagle Medium supplemented with 10% FBEssence and 1% penicillin−streptomycin; 5×10^5 cells were seeded onto glass bottom dishes 1 day prior to experiment. The cells were incubated with 200 nM of fluorescent VLPs for 4 h. The cells were washed 3× with HBSS, stained with 300 nM Hoescht 33442 dye for 10 min at 37 °C in HBSS, and washed again 3× with HBSS. The cells were kept in 1 mL of clean supplemented media for live-cell imaging using an Olympus FV3000 RS Confocal microscope. Both the GFP and the Cy5 lasers were used at the same power for imaging. The images from the individual filter sets were overlaid using ImageJ software. Z-stack 3D projections were also made with ImageJ.

Noninvasive Fluorescence Studies of smURFP@VLPs In Vivo. The following experiment was approved by the UT Dallas IACUC committee under protocol #18−17. All mice were fed a nonfluorescent diet and shaved to remove autofluorescence of hair. Mice were separated into 4 groups (n = 3) and injected either subcutaneously or intravenously (iv) with saline, smURFP (n), S@Qβ, or S@PP7—the VLP-containing solutions were prepared to ensure up to 100 μg was injected per mouse. All samples were set to have equal amounts of smURFP before injection. For subcutaneous injections, mice were monitored before and after injection at 1, 4, and 8 h. These experiments were repeated with different mice for the iv injections, except time points were taken before and after injection at 30 min, 1 h, and 2 h, and the mice were sacrificed at 2 h.

Radiance Efficiency Calculation via Ex Vivo Fluorescence Imaging. Intravenously injected BALB/c mice were sacrificed after 2 h of systematic smURFP and S@VLPs administration. Organs were harvested and imaged under an IVIS Lumina III at an excitation of 620 nm and emission at 670 nm with a set exposure time of 2 s. Regions of interest were constructed for each organ imaged. Average fluorescence for each organ tested (n = 3) was used for construction of a comparison plot between each of the samples injected. Mice injected with PBS were used as the control. In a similar experiment, mice were injected intravenously with S@Qβ and S@PP7 (Up to 100 μg) and the biodistribution recorded for 16 h. Mice were then sacrificed, major organs were extracted, and their fluorescence intensity was recorded.

■ ASSOCIATED CONTENT

Supporting Information

The Supporting Information is available free of charge at https://pubs.acs.org/doi/10.1021/acs.bioconjchem.0c00190.

Instrumentation and supplementary figures (PDF)

■ AUTHOR INFORMATION

Corresponding Author

Jeremiah J. Gassensmith − *Department of Chemistry and Biochemistry and Department of Bioengineering, The University of Texas at Dallas, Richardson, Texas 75080, United States;* orcid.org/0000-0001-6400-8106; Email: Gassensmith@utdallas.edu

Authors

Fabian C. Herbert − *Department of Chemistry and Biochemistry, The University of Texas at Dallas, Richardson, Texas 75080, United States*

Olivia R. Brohlin − *Department of Chemistry and Biochemistry, The University of Texas at Dallas, Richardson, Texas 75080, United States;* orcid.org/0000-0003-3226-6711

Tyler Galbraith − *Department of Chemistry and Biochemistry, The University of Texas at Dallas, Richardson, Texas 75080, United States*

Candace Benjamin − *Department of Chemistry and Biochemistry, The University of Texas at Dallas, Richardson, Texas 75080, United States*

Cesar A. Reyes − *Department of Chemistry and Biochemistry, The University of Texas at Dallas, Richardson, Texas 75080, United States*

Michael A. Luzuriaga − *Department of Chemistry and Biochemistry, The University of Texas at Dallas, Richardson, Texas 75080, United States;* orcid.org/0000-0001-6128-8800

Arezoo Shahrivarkevishahi − *Department of Chemistry and Biochemistry, The University of Texas at Dallas, Richardson, Texas 75080, United States*

Complete contact information is available at: https://pubs.acs.org/10.1021/acs.bioconjchem.0c00190

Author Contributions

Primary manuscript writing and editing was done by Fabian C. Herbert, Olivia R. Brohlin, and Jeremiah J. Gassensmith. Gel electrophoresis, SEC, DLS, UV−vis, mouse injections, and ex vivo studies were done by Fabian C. Herbert. Live-cell imaging and SEM were done by Olivia R. Brohlin. Production of fluorescent VLPs was done by Tyler Galbraith. Expression and purification of smURFP and GFP was done by Candace E. Benjamin. Expression and purification of Qβ and PP7 was done by Cesar A. Reyes. Mouse preparation prior to in vivo studies was performed by Michael A. Luzuriaga. Fluorescence spectroscopy was performed by Arezoo Shahrivarkevishahi. Funding was raised by Jeremiah J. Gassensmith.

Funding

J.J.G. thanks the National Science Foundation [CAREER DMR-1654405] and the Welch Foundation [AT-1989-20190330]. C.E.B. thanks the National Science Foundation Graduate Research Fellows Program (1746053).

Notes

The authors declare no competing financial interest.

■ ACKNOWLEDGMENTS

We thank Professor M. G. Finn and Dr. Po-Yu Fang for their helpful discussion and insight as well as the gift of the plasmids. We also thank Professor Erik A Rodriguez for helpful discussions.

■ REFERENCES

(1) Chen, Z., Li, N., Li, S., Dharmarwardana, M., Schlimme, A., and Gassensmith, J. J. (2016) Viral chemistry: The Chemical Functionalization of Viral Architectures to Create New Technology. *Wiley Interdiscip. Rev.: Nanomed. Nanobiotechnol. 8* (4), 512−534.

(2) Dharmarwardana, M., Martins, A. F., Chen, Z., Palacios, P. M., Nowak, C. M., Welch, R. P., Li, S., Luzuriaga, M. A., Bleris, L., Pierce,

B. S., et al. (2018) Nitroxyl Modified Tobacco Mosaic Virus as a Metal-free High-Relaxivity MRI and EPR Active Superoxide Sensor. *Mol. Pharmaceutics 15* (8), 2973−2983.
(3) Lee, H., Shahrivarkevishahi, A., Lumata, J. L., Luzuriaga, M. A., Hagge, L. M., Benjamin, C. E., Brohlin, O. R., Parish, C. R., Firouzi, H. R., Nielsen, S. O., et al. (2020) Supramolecular and Biomacromolecular Enhancement of Metal-free Magnetic Resonance Imaging Contrast Agents. *Chem. Sci. 11* (8), 2045−2050.
(4) Chen, Z., Li, N., Chen, L., Lee, J., and Gassensmith, J. J. (2016) Dual Functionalized Bacteriophage Qbeta as a Photocaged Drug Carrier. *Small 12* (33), 4563−4571.
(5) Welch, R. P., Lee, H., Luzuriaga, M. A., Brohlin, O. R., and Gassensmith, J. J. (2018) Protein−Polymer Delivery: Chemistry from the Cold Chain to the Clinic. *Bioconjugate Chem. 29* (9), 2867−2883.
(6) Lee, H., Benjamin, C. E., Nowak, C. M., Tuong, L. H., Welch, R. P., Chen, Z., Dharmarwardana, M., Murray, K. W., Bleris, L., D'Arcy, S., and Gassensmith, J. J. (2018) Regulating the Uptake of Viral Nanoparticles in Macrophage and Cancer Cells via a pH Switch. *Mol. Pharmaceutics 15* (8), 2984−2990.
(7) Benjamin, C. E., Chen, Z., Kang, P., Wilson, B. A., Li, N., Nielsen, S. O., Qin, Z., and Gassensmith, J. J. (2018) Site-Selective Nucleation and Size Control of Gold Nanoparticle Photothermal Antennae on the Pore Structures of a Virus. *J. Am. Chem. Soc. 140* (49), 17226−17233.
(8) Aniagyei, S. E., Dufort, C., Kao, C. C., and Dragnea, B. (2008) Self-assembly Approaches to Nanomaterial Encapsulation in Viral Protein Cages. *J. Mater. Chem. 18* (32), 3763−3774.
(9) Luzuriaga, M. A., Welch, R. P., Dharmarwardana, M., Benjamin, C. E., Li, S., Shahrivarkevishahi, A., Popal, S., Tuong, L. H., Creswell, C. T., and Gassensmith, J. J. (2019) Enhanced Stability and Controlled Delivery of MOF-Encapsulated Vaccines and Their Immunogenic Response In Vivo. *ACS Appl. Mater. Interfaces 11* (10), 9740−9746.
(10) Murray, A. A., Sheen, M. R., Veliz, F. A., Fiering, S. N., and Steinmetz, N. F. (2019) In Situ Vaccination of Tumors Using Plant Viral Nanoparticles. *Methods Mol. Biol. 2000*, 111−124.
(11) Wang, C., Beiss, V., and Steinmetz, N. F. (2019) Cowpea Mosaic Virus Nanoparticles and Empty Virus-Like Particles Show Distinct but Overlapping Immunostimulatory Properties. *J. Virol. 93* (21), No. e00129-19.
(12) Li, S., Dharmarwardana, M., Welch, R. P., Benjamin, C. E., Shamir, A. M., Nielsen, S. O., and Gassensmith, J. J. (2018) Investigation of Controlled Growth of Metal−Organic Frameworks on Anisotropic Virus Particles. *ACS Appl. Mater. Interfaces 10* (21), 18161−18169.
(13) Lee, P. W., Shukla, S., Wallat, J. D., Danda, C., Steinmetz, N. F., Maia, J., and Pokorski, J. K. (2017) Biodegradable Viral Nanoparticle/Polymer Implants Prepared via Melt-Processing. *ACS Nano 11* (9), 8777−8789.
(14) Rynda-Apple, A., Patterson, D. P., and Douglas, T. (2014) Virus-Like Particles as Antigenic Nanomaterials for Inducing Protective Immune Responses in the Lung. *Nanomedicine 9* (12), 1857−1868.
(15) Zhao, L., Kopylov, M., Potter, C. S., Carragher, B., and Finn, M. G. (2019) Engineering the PP7 Virus Capsid as a Peptide Display Platform. *ACS Nano 13* (4), 4443−4454.
(16) Liu, J., Dai, S., Wang, M., Hu, Z., Wang, H., and Deng, F. (2016) Virus Like Particle-Based Vaccines Against Emerging Infectious Disease Viruses. *Virol. Sin. 31* (4), 279−287.
(17) Pokorski, J. K., Hovlid, M. L., and Finn, M. G. (2011) Cell Targeting with Hybrid Qβ Virus-Like Particles Displaying Epidermal Growth Factor. *ChemBioChem 12* (16), 2441−2447.
(18) Prasuhn, D. E., Jr., Singh, P., Strable, E., Brown, S., Manchester, M., and Finn, M. G. (2008) Plasma Clearance of Bacteriophage Qβ Particles as a Function of Surface Charge. *J. Am. Chem. Soc. 130* (4), 1328−1334.
(19) Chen, Z., Boyd, S. D., Calvo, J. S., Murray, K. W., Mejia, G. L., Benjamin, C. E., Welch, R. P., Winkler, D. D., Meloni, G., D'Arcy, S., et al. (2017) Fluorescent Functionalization Across Quaternary Structure in a Virus-Like Particle. *Bioconjugate Chem. 28* (9), 2277−2283.
(20) Dharmarwardana, M., Martins, A. F., Chen, Z., Palacios, P. M., Nowak, C. M., Welch, R. P., Li, S., Luzuriaga, M. A., Bleris, L., Pierce, B. S., et al. (2018) Nitroxyl Modified Tobacco Mosaic Virus as a Metal-Free High-Relaxivity MRI and EPR Active Superoxide Sensor. *Mol. Pharmaceutics 15* (8), 2973−2983.
(21) Chen, C. C., Stark, M., Baikoghli, M., and Cheng, R. H. (2018) Surface Functionalization of Hepatitis E Virus Nanoparticles Using Chemical Conjugation Methods. *J. Visualized Exp. 135*, No. e57020.
(22) Sainsbury, F., Saunders, K., Aljabali, A. A., Evans, D. J., and Lomonossoff, G. P. (2011) Peptide-controlled Access to the Interior Surface of Empty Virus Nanoparticles. *ChemBioChem 12* (16), 2435−2440.
(23) Steinmetz, N. F. (2010) Viral Nanoparticles as Platforms for Next-generation Therapeutics and Imaging Devices. *Nanomedicine 6* (5), 634−641.
(24) Nanduri, V., Balasubramanian, S., Sista, S., Vodyanoy, V. J., and Simonian, A. L. (2007) Highly Sensitive Phage-based Biosensor for the Detection of Beta-galactosidase. *Anal. Chim. Acta 589* (2), 166−172.
(25) Robertson, K. L., and Liu, J. L. (2012) Engineered Viral Nanoparticles for Flow Cytometry and Fluorescence Microscopy Applications. *Wiley Interdiscip. Rev. Nanomed. Nanobiotechnol. 4* (5), 511−524.
(26) Lewis, J. D., Destito, G., Zijlstra, A., Gonzalez, M. J., Quigley, J. P., Manchester, M., and Stuhlmann, H. (2006) Viral nanoparticles as tools for intravital vascular imaging. *Nat. Med. 12* (3), 354−360.
(27) Carrico, Z. M., Farkas, M. E., Zhou, Y., Hsiao, S. C., Marks, J. D., Chokhawala, H., Clark, D. S., and Francis, M. B. (2012) N-Terminal Labeling of Filamentous Phage to Create Cancer Marker Imaging Agents. *ACS Nano 6* (8), 6675−6680.
(28) Benjamin, C. E., Chen, Z., Brohlin, O. R., Lee, H., Shahrivarkevishahi, A., Boyd, S., Winkler, D. D., and Gassensmith, J. J. (2020) Using FRET to Measure the Time it Takes for a Cell to Destroy a Virus. *Nanoscale 12*, 9124.
(29) Jaffe, J., Wucherer, K., Sperry, J., Zou, Q., Chang, Q., Massa, M. A., Bhattacharya, K., Kumar, S., Caparon, M., Stead, D., et al. (2019) Effects of Conformational Changes in Peptide-CRM197 Conjugate Vaccines. *Bioconjugate Chem. 30* (1), 47−53.
(30) Rhee, J. K., Hovlid, M., Fiedler, J. D., Brown, S. D., Manzenrieder, F., Kitagishi, H., Nycholat, C., Paulson, J. C., and Finn, M. G. (2011) Colorful Virus-like Particles: Fluorescent Protein Packaging by the Qbeta capsid. *Biomacromolecules 12* (11), 3977−3981.
(31) Minten, I. J., Claessen, V. I., Blank, K., Rowan, A. E., Nolte, R. J. M., and Cornelissen, J. J. L. M. (2011) Catalytic Capsids: The Art of Confinement. *Chem. Sci. 2* (2), 358−362.
(32) Luker, K. E., Pata, P., Shemiakina, II, Pereverzeva, A., Stacer, A. C., Shcherbo, D. S., Pletnev, V. Z., Skolnaja, M., Lukyanov, K. A., Luker, G. D., et al. (2015) Comparative Study Reveals Better Far-red Fluorescent Protein for Whole Body Imaging. *Sci. Rep. 5*, 10332.
(33) Smith, A. M., Mancini, M. C., and Nie, S. (2009) Bioimaging: Second Window for *in vivo* Imaging. *Nat. Nanotechnol. 4* (11), 710−711.
(34) Shcherbakova, D. M., Subach, O. M., and Verkhusha, V. V. (2012) Red Fluorescent Proteins: Advanced Imaging Applications and Future Design. *Angew. Chem., Int. Ed. 51* (43), 10724−10738.
(35) Morozova, K. S., Piatkevich, K. D., Gould, T. J., Zhang, J., Bewersdorf, J., and Verkhusha, V. V. (2010) Far-red Fluorescent Protein Excitable with Red Lasers for Flow Cytometry and Superresolution STED Nanoscopy. *Biophys. J. 99* (2), L13−5.
(36) Wang, L., Jackson, W. C., Steinbach, P. A., and Tsien, R. Y. (2004) Evolution of New Nonantibody Proteins via Iterative Somatic Hypermutation. *Proc. Natl. Acad. Sci. U. S. A. 101* (48), 16745−16749.
(37) Rodriguez, E. A., Tran, G. N., Gross, L. A., Crisp, J. L., Shu, X., Lin, J. Y., and Tsien, R. Y. (2016) A Far-red Fluorescent Protein

https://dx.doi.org/10.1021/acs.bioconjchem.0c00190
Bioconjugate Chem. 2020, 31, 1529−1536

Evolved from a Cyanobacterial Phycobiliprotein. *Nat. Methods 13* (9), 763−769.
(38) Oliinyk, O. S., Chernov, K. G., and Verkhusha, V. V. (2017) Bacterial Phytochromes, Cyanobacteriochromes and Allophycocyanins as a Source of Near-Infrared Fluorescent Probes. *Int. J. Mol. Sci. 18* (8), 1691.
(39) An, F., Chen, N., Conlon, W. J., Hachey, J. S., Xin, J., Aras, O., Rodriguez, E. A., and Ting, R. (2020) Small Ultra-red Fluorescent Protein Nanoparticles as Exogenous Probes for Noninvasive Tumor Imaging In Vivo. *Int. J. Biol. Macromol. 153*, 100−106.
(40) Shaner, N. C., Campbell, R. E., Steinbach, P. A., Giepmans, B. N., Palmer, A. E., and Tsien, R. Y. (2004) Improved Monomeric Red, Orange and Yellow Fluorescent Proteins Derived from Discosoma Sp. Red Fluorescent Protein. *Nat. Biotechnol. 22* (12), 1567−1572.
(41) Kredel, S., Nienhaus, K., Oswald, F., Wolff, M., Ivanchenko, S., Cymer, F., Jeromin, A., Michel, F. J., Spindler, K. D., Heilker, R., et al. (2008) Optimized and Far-red-emitting Variants of Fluorescent Protein eqFP611. *Chem. Biol. 15* (3), 224−233.
(42) Shcherbo, D., Merzlyak, E. M., Chepurnykh, T. V., Fradkov, A. F., Ermakova, G. V., Solovieva, E. A., Lukyanov, K. A., Bogdanova, E. A., Zaraisky, A. G., Lukyanov, S., et al. (2007) Bright Far-red Fluorescent Protein for Whole-body Imaging. *Nat. Methods 4* (9), 741−746.
(43) Oliinyk, O. S., Shemetov, A. A., Pletnev, S., Shcherbakova, D. M., and Verkhusha, V. V. (2019) Smallest Near-infrared Fluorescent Protein Evolved from Cyanobacteriochrome as Versatile Tag for Spectral Multiplexing. *Nat. Commun. 10* (1), 279.
(44) Capehart, S. L., Coyle, M. P., Glasgow, J. E., and Francis, M. B. (2013) Controlled Integration of Gold Nanoparticles and Organic Fluorophores Using Synthetically Modified MS2 Viral Capsids. *J. Am. Chem. Soc. 135* (8), 3011−3016.
(45) Glasgow, J. E., Capehart, S. L., Francis, M. B., and Tullman-Ercek, D. (2012) Osmolyte-mediated Encapsulation of Proteins Inside MS2 Viral Capsids. *ACS Nano 6* (10), 8658−8664.
(46) Lavelle, L., Michel, J.-P., and Gingery, M. (2007) The disassembly, reassembly and stability of CCMV protein capsids. *J. Virol. Methods 146* (1), 311−316.
(47) Azuma, Y., Edwardson, T. G. W., and Hilvert, D. (2018) Tailoring lumazine synthase assemblies for bionanotechnology. *Chem. Soc. Rev. 47* (10), 3543−3557.
(48) Gysi, J. R., and Zuber, H. (1979) Properties of Allophycocyanin II and its Alpha- and Beta-subunits from the Thermophilic Blue–green Alga Mastigocladus Laminosus. *Biochem. J. 181* (3), 577−583.
(49) Chen, Z., Detvo, S. T., Pham, E., and Gassensmith, J. J. (2018) Making Conjugation-induced Fluorescent PEGylated Virus-like Particles by Dibromomaleimide-disulfide Chemistry. *J. Visualized Exp.* No. 135, No. e57712.
(50) Koudelka, K. J., Pitek, A. S., Manchester, M., and Steinmetz, N. F. (2015) Virus-Based Nanoparticles as Versatile Nanomachines. *Annu. Rev. Virol. 2* (1), 379−401.
(51) Schwarz, B., Uchida, M., and Douglas, T. (2017) Biomedical and Catalytic Opportunities of Virus-Like Particles in Nanotechnology. *Adv. Virus Res. 97*, 1−60.
(52) Sun, J., DuFort, C., Daniel, M.-C., Murali, A., Chen, C., Gopinath, K., Stein, B., De, M., Rotello, V. M., Holzenburg, A., et al. (2007) Core-controlled Polymorphism in Virus-like Particles. *Proc. Natl. Acad. Sci. U. S. A. 104* (4), 1354−1359.
(53) Liu, A., de Ruiter, M. V., Zhu, W., Maassen, S. J., Yang, L., and Cornelissen, J. J. L. M. (2018) Compartmentalized Thin Films with Customized Functionality via Interfacial Cross-linking of Protein Cages. *Adv. Funct. Mater. 28* (34), 1801574.
(54) Ding, W. L., Miao, D., Hou, Y. N., Jiang, S. P., Zhao, B. Q., Zhou, M., Scheer, H., and Zhao, K. H. (2017) Small Monomeric and Highly Stable Near-infrared Fluorescent Markers Derived from the Thermophilic Phycobiliprotein, ApcF2. *Biochim. Biophys. Acta, Mol. Cell Res. 1864* (10), 1877−1886.
(55) Kneen, M., Farinas, J., Li, Y., and Verkman, A. S. (1998) Green Fluorescent Protein as a Noninvasive Intracellular pH Indicator. *Biophys. J. 74* (3), 1591−1599.
(56) The authors appreciate that there is some variation in the efficiency of the filter sets, and while the same laser power was used, we understand that this is difficult to control without measuring photon flux. We did our level best to ensure identical conditions during imaging with both GFP- and smURFP-based probes; however, the real proof is simply seeing the probes in action during live-cell imaging. The difference in how easy it is to obtain quality images is considerable.
(57) Herbert, F. C., Brohlin, O., Galbraith, T., Benjamin, C., Reyes, C., Luzuriaga, M. A., Shahrivarkevishahi, A., and Gassensmith, J. J Supramolecular Encapsulation of Small-Ultra Red Fluorescent Proteins in Virus-Like Nanoparticles for Non-Invasive In Vivo Imaging Agents. *Bioconjugate Chem.* 2020 DOI: 10.1021/acs.bioconjchem.0c00190